Soliton triads ensemble in frequency conversion: from inverse scattering theory to experimental observation

Fabio Baronio, Marco Andreana, Matteo Conforti, Gabriele Manili, Vincent Couderc, Costantino de Angelis, Alain Barthélémy

Soliton triads ensemble in frequency conversion: from inverse scattering theory to experimental observation

Fabio Baronio,[1,*] **Marco Andreana,**[2] **Matteo Conforti,**[1] **Gabriele Manili,**[1] **Vincent Couderc,**[2] **Costantino De Angelis,**[1] **and Alain Barthélémy**[2]

[1]*CNISM, Dipartimento di Ingegneria dell'Informazione, Università di Brescia, Via Branze 38, 25123 Brescia, Italy*

[2]*XLIM Research Institute, Centre National de la Recherche Scientifique, University of Limoges, Av. Albert Thomas 123, 87060, Limoges, France*

[*]*fabio.baronio@ing.unibs.it*

Abstract: We consider the spectral theory of three–wave interactions to predict the initiation, formation and dynamics of an ensemble of bright–dark–bright soliton triads in frequency conversion processes. Spatial observation of non–interacting triads ensemble in a KTP crystal confirms theoretical prediction and numerical simulations.

OCIS codes: (190.5530) Pulse propagation and solitons; (190.2620) Frequency conversion; (190.4410) Nonlinear optics, parametric processes.

References and links

1. D. J. Kaup, A. Reiman, and A. Bers, "Space-time evolution of nonlinear three-wave interactions. I. interaction in a homogeneous medium," Rev. Mod. Phys. **51,** 275–309 (1979).
2. V. E. Zakharov and S. V. Manakov, "Resonant interaction of wave packets in nonlinear media," JETP Lett. **18,** 243–245 (1973).
3. V. E. Zakharov, *What is Integrability?* (Springer-Verlag, 1991).
4. A. Hasegawa, *Plasma Instabilities and Nonlinear Effects* (Springer-Verlag, 2001).
5. W. Cheng, Y. Avitzour, Y. Ping, S. Suckewer, N. Fisch, M. Hur, and J. Wurtele, "Reaching the nonlinear regime of raman amplification of ultrashort laser pulses," Phys. Rev. Lett. **94,** 045003 (2005).
6. E. Ibragimov and A. Struthers, "Second harmonic pulse compression in the soliton regime," Opt. Lett. **21,** 1582–1584 (1996).
7. A. Picozzi and M. Haelterman, "Spontaneous formation of symbiotic solitary waves in a backward quasi-phase-matched parametric oscillator," Opt. Lett. **23,** 1808–1810 (1998).
8. A. Degasperis, M. Conforti, F. Baronio, and S. Wabnitz, "Stable control of pulse speed in parametric three-wave solitons," Phys. Rev. Lett. **97,** 093901 (2006).
9. M. Conforti, F. Baronio, A. Degasperis, and S. Wabnitz, "Parametric frequency conversion of short optical pulses controlled by a CW background," Opt. Express **15,** 12246–12251 (2007).
10. A. Craik, *Wave Interactions and Fluid Flows* (Cambridge Univ. Press, 1985).
11. K. Lamb, "Tidally generated near-resonant internal wave triads at shelf break," Geophys. Res. Lett. **34,** L18607 (2007).
12. E. Segre, *Collected Papers of Enrico Fermi* (University of Chicago Press, 1965).
13. J. Ibanez and E. Verdaguer, "Soliton collision in general-relativity," Phys. Rev. Lett. **51,** 1313 (1983).
14. A. R. Osborne, M. Onorato, M. Serio, and L. Bergamasco, "Soliton creation and destruction, resonant interactions, and inelastic collisions in shallow water waves," Phys. Rev. Lett. **81,** 3559 (1998).
15. B. Damski and W. Zurek, "Soliton creation during a Bose-Einstein Condensation," Phys. Rev. Lett. **104,** 160404 (2010).
16. Y. S. Kivshar and G. P. Agrawal, *Optical Solitons: from Fibers to Photonic Crystals* (Academic Press, 2003).

#144063 - $15.00 USD Received 11 Mar 2011; revised 9 May 2011; accepted 26 May 2011; published 23 Jun 2011

17. C. Conti, A. Fratalocchi, M. Peccianti, G. Ruocco, S. Trillo, "Observation of a gradient catastrophe generating solitons," Phys. Rev. Lett. **102,** 083902 (2009).
18. K. Nozaki and T. Taniuti, "Propagation of solitary pulses in interactions of plasma waves," J. Phys. Soc. Jpn. **34,** 796–800 (1973).
19. A. Abdolvand, A. Nazarkin, A. Chugreev, C. Kaminski, P. Russel, "Solitary pulse generation by backward raman scattering in H-2-filled photonic crystal fibers," Phys. Rev. Lett. **103,** 183902 (2009).
20. F. Baronio, M. Conforti, M. Andreana, V. Couderc, C. De Angelis, S. Wabnitz, A.Barthelemy, and A. Degasperis, "Frequency generation and solitonic decay in three wave interactions," Opt. Express **17,** 13889–13894 (2009).
21. F. Baronio, M. Conforti, C. De Angelis, A. Degasperis, M. Andreana, V. Couderc, A. Barthelemy, "Velocity-locked solitary waves in quadratic media," Phys. Rev. Lett **104,** 113902 (2010).
22. A. Degasperis, M. Conforti, F. Baronio, S. Wabnitz, S. Lombardo, "The three-wave resonant interaction equations: spectral and numerical methods," Lett. Math. Phys. **96,** 367 (2011).
23. M. Conforti, F. Baronio, A. Degasperis, S. Wabnitz, "Inelastic scattering and interactions of three-wave parametric solitons," Phys. Rev. E **74,** 065602 (2006).
24. A. Fratalocchi, C. Conti, G. Ruocco, S. Trillo "Free-energy transition in a gas of noninteracting nonlinear wave particles," Phys. Rev. Lett. **101,** 044101 (2008).

1. Introduction

Three-wave interactions (TWIs) describe the resonant mixing of waves in weakly nonlinear media. The TWI model is typically encountered in the description of any conservative nonlinear medium where the dynamics can be considered as a perturbation of the linear wave solution, the lowest-order nonlinearity is quadratic in the field amplitudes, and the phase-matching (or resonance) condition is satisfied [1]. The TWI model possesses two important properties, namely it is universal and integrable [2, 3]. Universality implies that TWI is ubiquitous in various branches of science: indeed, TWI has been applied in plasma physics, fluid dynamics, optics, acoustics [1, 4–11]. The second TWI feature, integrability, gives mathematical tools to investigate several problems such as the evolution of given initial data, construction of particular analytic solutions (f.i. solitons) and the derivation of (infinitely many) conservation laws. Indeed, stemming from the numerical experiments of Fermi-Pasta-Ulam on the equipartition of energy in nonlinear chains [12], solitons have found significant applications in areas as different as general relativity, oceanography, Bose-Einstein condensation, photonics [13–17]. Solitons behave like particles, conserve their number and spectral parameters (eigenvalues) and keep their identity upon interactions, the only effect being some displacements after their collisions. The spectral invariance allows for reducing the infinito-dimensional phase space associated with the global wave functions to simple ones where N independent degrees of freedom corresponding to N soliton particles are effective. TWI soliton has been predicted in the 70s [1, 18], and recently observed in photonic crystal fibers [19] and in quadratic crystals [20, 21].

In this Letter, we consider spatial coherent optical TWIs in a lossless quadratic medium. We study the dynamics of a spatial narrow beam at frequency ω_1 (the signal) and a quasi-plane wave at frequency ω_2 (the pump) which mix to generate a beam at the sum frequency (SF) ω_3 (the idler), when diffraction is negligible. Depending on the input intensities different nonlinear regimes exist: frequency conversion, single soliton triad generation, N–soliton triads ensemble. Frequency conversion: the signal and pump beams interact and generate an idler beam whose spatial characteristics are associated with the interaction distance in the crystal; signal and pump are depleted. Soliton triad generation: the signal and pump beams interact, generate a stable symbiotic bright-dark-bright triplet moving with a locked spatial nonlinear walk–off [8, 21]. N–soliton triads ensemble: the signal and pump input beams generate N soliton triads moving with different spatial nonlinear walk-offs. In this Letter, the focus is on the generation and dynamics of an ensemble of TWI soliton triads. We obtain the results by a complementary use of spectral theory (inverse scattering transform, IST), numerical integration of the TWI equations, and experiments in nonlinear optics.

#144063 - $15.00 USD Received 11 Mar 2011; revised 9 May 2011; accepted 26 May 2011; published 23 Jun 2011

2. TWI equations and inverse scattering

Three quasi monochromatic waves with wave–numbers k_1 , k_2 , k_3 and frequencies ω_1 , ω_2 , ω_3, which propagate in a nonlinear optical medium, interact efficiently with each other and exchange energy if the resonance conditions $k_1+k_2=k_3$, $\omega_1+\omega_2=\omega_3$, are satisfied. The equations describing spatial interaction of beams read [21]:

$$\begin{aligned}
\Big(\frac{\partial}{\partial z}+\rho_1\frac{\partial}{\partial x}\Big)E_1+\frac{1}{2ik_1}\Big(\frac{\partial^2}{\partial x^2}+\frac{\partial^2}{\partial y^2}\Big)E_1 &= i\chi_1E_2^*E_3,\\
\Big(\frac{\partial}{\partial z}+\rho_2\frac{\partial}{\partial x}\Big)E_2+\frac{1}{2ik_2}\Big(\frac{\partial^2}{\partial x^2}+\frac{\partial^2}{\partial y^2}\Big)E_2 &= i\chi_2E_1^*E_3,\\
\Big(\frac{\partial}{\partial z}+\rho_3\frac{\partial}{\partial x}\Big)E_3+\frac{1}{2ik_3}\Big(\frac{\partial^2}{\partial x^2}+\frac{\partial^2}{\partial y^2}\Big)E_3 &= i\chi_3E_1E_2.
\end{aligned} \tag{1}$$

$E_n(x,y,z)$ are the slowly varying electric field envelopes of the waves at frequencies ω_j (wavelength λ_j), $k_n=\omega_n\mathtt{n}_n/c$ are the wavenumbers, $\mathtt{n}_n$ the refractive indexes, $\chi_n=2d\omega_j/c\mathtt{n}_n$ the nonlinear coupling coefficients (d is the quadratic nonlinear susceptibility and c is the speed of light), ρ_j the walk off angles, $n=1,2,3$. z is the spatial longitudinal propagation coordinate, x and y are the spatial transverse coordinates. In the case of negligible diffraction, Eqs. (1) can be mapped into adimensional TWI equations:

$$\begin{aligned}
\left(\frac{\partial}{\partial\xi}+\delta_1\frac{\partial}{\partial s}\right)\phi_1 &= i\phi_2^*\phi_3,\\
\left(\frac{\partial}{\partial\xi}+\delta_2\frac{\partial}{\partial s}\right)\phi_2 &= i\phi_1^*\phi_3,\\
\left(\frac{\partial}{\partial\xi}+\delta_3\frac{\partial}{\partial s}\right)\phi_3 &= i\phi_1\phi_2,
\end{aligned} \tag{2}$$

where $\phi_n=E_nz_0\sqrt{\chi_{n+1}\chi_{n+3}}, n=1,2,3\ mod\,3$, $\delta_n=\rho_nz_0/x_0$, $\xi=z/z_0, s=x/x_0$, with z_0,x_0 longitudinal and transverse scale lengths, respectively. Diffraction becomes negligible when $z_0/(k_nx_0^2)<<1$.

For purpose of the IST, it is convenient to transform Eqs. (2) to more symmetric equations. Let $Q_{1,3}=\phi_{1,2}e^{-i\pi/6}$, $Q_2=\phi_3^*e^{-i\pi/6}$, $\nu_1=\delta_1$, $\nu_{2,3}=\delta_{3,2}$ and $(\sigma_1\,,\sigma_2\,,\sigma_3)=(+\,,-\,,+)$. Equations (2) turn out to be:

$$\left(\frac{\partial}{\partial\xi}+\nu_n\frac{\partial}{\partial s}\right)Q_n=\sigma_nQ_{n+1}^*Q_{n+2}^* \quad n=1,2,3,mod3. \tag{3}$$

The integrability of Eqs. (3) follows from the fact that these equations are the compatibility conditions of two 3×3 matrix ordinary differential equations (ODEs), one in the variable s and the other one in ξ (the Zakharov–Manakov eigenvalue problem [2]). This fact gives a way to set up a nonlinear generalization of the Fourier analysis of solutions of the associated initial value problem, namely the IST. In particular, this generalization leads to decompose a given solution $Q_1(s,\xi)\,,Q_2(s,\xi)\,,Q_3(s,\xi)$ as functions of s at a given fixed ξ in its continuum spectrum component (radiation) and in discrete spectrum component (solitons). This pair of equations (the Lax pair) reads [22]

$$\psi_s=[i\lambda A+E(s,\xi)]\psi\,, \tag{4}$$

$$\psi_\xi=[i\lambda B+F(s,\xi)]\psi+\psi C\,, \tag{5}$$

#144063 - $15.00 USD Received 11 Mar 2011; revised 9 May 2011; accepted 26 May 2011; published 23 Jun 2011

where $\psi = \psi(s,\xi,\lambda)$ is a 3–dimensional vector solution, λ is the complex spectral variable and C is a constant matrix which depends on the boundary conditions on the s-axis. A and B are constant real and traceless diagonal matrices, $A = \mathrm{diag}\{a_1, a_2, a_3\}$, $B = \mathrm{diag}\{b_1, b_2, b_3\}$ whose entries are $a_n = 2\nu_n - \nu_{n+1} - \nu_{n+2}$, $b_n = 2\nu_{n+1}\nu_{n+2} - \nu_n(\nu_{n+1} + \nu_{n+2})$, $n = 1,2,3 \bmod 3$, while the three wave fields Q_n enter in the matrices $E(s,\xi)$ and $F(s,\xi)$ through the expressions:

$$E = \begin{pmatrix} 0 & u_3 & v_2 \\ v_3 & 0 & u_1 \\ u_2 & v_1 & 0 \end{pmatrix}, \; F = -\begin{pmatrix} 0 & v_3 u_3 & v_2 v_2 \\ v_3 v_3 & 0 & v_1 u_1 \\ v_2 u_2 & v_1 v_1 & 0 \end{pmatrix}, \tag{6}$$

where $u_n = \sigma_n w \sqrt{(-1)^n(\nu_{n+1} - \nu_{n+2})} Q_n$, $\nu_n = (-1)^{n+1}\sigma w \sqrt{(-1)^n(\nu_{n+1} - \nu_{n+2})} Q_n^*$, $\sigma = \sigma_1\sigma_2\sigma_3$, $w = [(\nu_3 - \nu_1)(\nu_2 - \nu_1)(\nu_3 - \nu_2)]^{-1/2}$, $n = 1,2,3 \bmod 3$.

Similarly to solving linear partial differential equations (PDEs) by using the Fourier transform, the scheme to follow here to solve the TWI Eqs. (2) with given initial data $\phi_n(s,\xi_0)$ is:

1. computing the spectral data associated with $Q_n(s,\xi_0)$ by integrating the ODE (Eq. (4)), i.e. solving the *direct* problem;
2. finding the spectral data at a different coordinate $\xi \neq \xi_0$, which usually reduces to a trivial multiplication for a phase factor;
3. recovering the solution $Q_n(s,\xi)$ at coordinate $\xi \neq \xi_0$ by solving the inverse problem, then $\phi_n(s,\xi)$.

The focus in the present work is on step (1), the determination of the eigenvalues and eigenfunctions in the direct problem, since in most applications the spectral data contain quite a relevant information, particularly the interest is on the discrete spectrum (the soliton content). Reference [22] reports a detailed description of both the spectral theory and the numerical algorithm used to solve the scattering problem.

3. Theoretical analysis

We investigate the evolution of beams ϕ_1, ϕ_2, ϕ_3 in the $s - \xi$ plane, given the initial condition $\phi_1(s,0) = \varepsilon_1 \mathrm{sech}(s)$, for the signal, $\phi_2(s,0) = \varepsilon_2[h(s_0 - s) + h(s - s_\infty)]$ ($h(s)$ is the Heaviside function, s_∞ is a large positive constant), for the pump, $\phi_3(s,0) = 0$, for the SF beam. We fix $\delta_1 = -2, \delta_2 = 0, \delta_3 = -1$, $s_0 = -6$, and we vary $\varepsilon_1, \varepsilon_2$ amplitudes. We assumed a non vanishing pump as $s \to +\infty$ to apply the numerical spectral method for non vanishing boundary conditions [22].

At low input amplitudes ($\varepsilon_1 = 0.5, \varepsilon_2 = 0.05$), the initial data are composed of a continuum spectrum component (radiation) and no discrete spectrum component (solitons). This regime corresponds to the well known optical non-collinear sum-frequency generation. Numerical simulations (Fig. 1) show that signal beam ϕ_1 and the pump beam ϕ_2 propagate with their own characteristic velocities; as long as the signal beam overtakes the pump beam, a idler beam ϕ_3 at the sum-frequency is generated which propagates with its own characteristic walk-off; indeed, the V shape of the idler beam is due to its intrinsic linear walk-off. Pump beam is deeply depleted.

Increasing input amplitudes ($\varepsilon_1 = 1.42, \varepsilon_2 = 0.7$), the initial data are composed of both a continuum spectrum component (radiation) and a discrete spectrum component (solitons). The input waves contain one soliton plus radiation. Figure 2(a) reports the initial envelope conditions, Fig. 2(b) shows the correspondent eignevalue $\lambda = 0.33i$ and eigenfunctions ψ_n. Through the spectral data we can predict the initiation of a bright-dark-bright triad and its properties (f.i.,

#144063 - $15.00 USD Received 11 Mar 2011; revised 9 May 2011; accepted 26 May 2011; published 23 Jun 2011

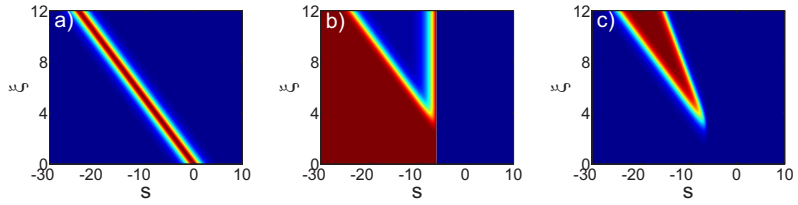

Fig. 1. Frequency conversion. Numerical dynamics of the beams ϕ_1 (a), ϕ_2 (b), ϕ_3 (c) in the $s-\xi$ plane.

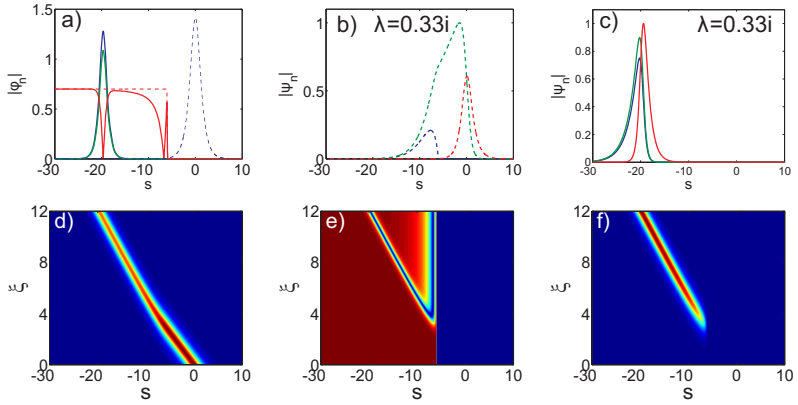

Fig. 2. Single-soliton triad generation. a) Beam profiles ϕ_1 (blue line), ϕ_2 (red line), ϕ_3 (green line) at input $\xi = 0$ (dashed lines) and at output $\xi = 12$ (solid lines). b) Eigenvalue λ and spectral eigenfunctions ψ_1 (blue line), ψ_2 (red line), ψ_3 (green line) corresponding to input data at $\xi = 0$. c) Spectral informations at $\xi = 12$. Numerical dynamics of the beams ϕ_1 (d), ϕ_2 (e), ϕ_3 (f) in the $s-\xi$ plane.

nonlinear walk-off, amplitudes, etc.). The relation between eigenvalues and soliton parameters can be found in Ref. [22]. Indeed, numerical simulations (Fig. 2(d)–2(f)) show that the interaction of the signal and pump beams leads to the generation of a stable bright-dark-bright solitary triplet moving with a locked nonlinear walk-off that lies in between the characteristic linear walk-offs of the signal and the idler, as observed in Ref. [21]. Figure 2(c) reports the spectral informations of the soliton triad at output $\xi = 12$. A similar phenomenon of soliton generation could be observed also for a smoother transition between zero and the pump level necessary to support the soliton.

Now, the key point is to argue whether, by increasing signal amplitude, a single high-intensity bright-dark-bright soliton or an ensemble of attractive, repulsive, or non-interacting soliton triplets would be excited in frequency conversion processes.

At higher signal amplitude and fixed pump amplitude ($\varepsilon_1 = 2.82, \varepsilon_2 = 0.7$), the initial data contain $N = 2$ stable soliton triads, with different nonlinear walk-offs, plus radiation. Figure 3(a)–3(c) report the initial conditions, the correspondent eigenvalues $\lambda_1 = 0.33i$, $\lambda_2 = i$ and eigenfunctions of the discrete spectrum. The stability of soliton triads can be characterized analytically as reported in Ref. [23]. Numerical simulations confirm that the interaction of the signal and pump beams leads to the initiation of two soliton bright-dark-bright triads which propagate with different spatial nonlinear walk-offs (Fig. 3(d)–3(f)). The first triad is exactly the

#144063 - $15.00 USD Received 11 Mar 2011; revised 9 May 2011; accepted 26 May 2011; published 23 Jun 2011

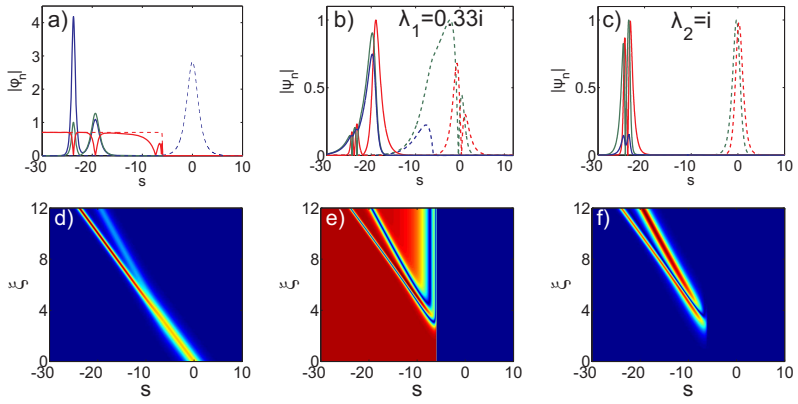

Fig. 3. Soliton triads. (a) Beam profiles ϕ_1 (blue line), ϕ_2 (red line), ϕ_3 (green line) at input $\xi = 0$ (dashed lines) and at output $\xi = 12$ (solid lines). (b)-(c) Eigenvalue λ and spectral eigenfunctions ψ_1 (blue line), ψ_2 (red line), ψ_3 (green line) corresponding to envelope input data at $\xi = 0$ (dashed lines) and $\xi = 12$ (solid lines). Numerical dynamics of the beams ϕ_1 (d), ϕ_2 (e), ϕ_3 (f) in the $s - \xi$ plane.

same of the previous case, albeit some displacements. The triads do not interact, do not attract, do not repel: in fact interaction would lead to the modification of the spectral characteristics (the eigenvalue) of the first triad. Increasing further input amplitudes ($\varepsilon_1 = 4.24, \varepsilon_2 = 0.75$), the

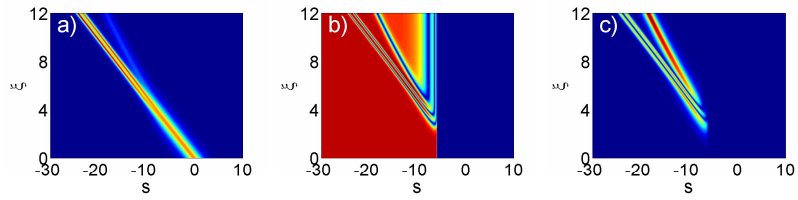

Fig. 4. Soliton triads. Numerical dynamics of the beams ϕ_1 (a), ϕ_2 (b), ϕ_3 (c) in the $s - \xi$ plane.

initial data contain $N = 3$ stable soliton triads. The correspondent eigenvalues are $\lambda_1 = 0.33i$, $\lambda_2 = i$ and $\lambda_3 = 1.66i$. Figure 4(a)–4(c) show the generation of three soliton bright-dark-bright triads.

The important result is that the signal beam at input can contain N bright solitons [1] moving with the linear walk-off δ_1 which reshape, after the interaction of the pump beam, in N *non-interacting* bright-dark-bright solitons triads [8] moving with different nonlinear walk–offs. Of course, it's fashinating to argue whether an ensemble of non-interacting soliton triads exhibit cooperative phenomena as the numbers of free particles grows (f.i., critical shock phenomena [24]).

4. Experimental investigation

The TWI soliton physics can be experimentally tested. In the experiments (see Fig. 5), a Q-switched laser, combined with a temporal passive compression system, delivers $150ps$ pulses at $\lambda = 1064nm$. We introduce a Glan polarizer to obtain, after passage of the light through

#144063 - $15.00 USD Received 11 Mar 2011; revised 9 May 2011; accepted 26 May 2011; published 23 Jun 2011

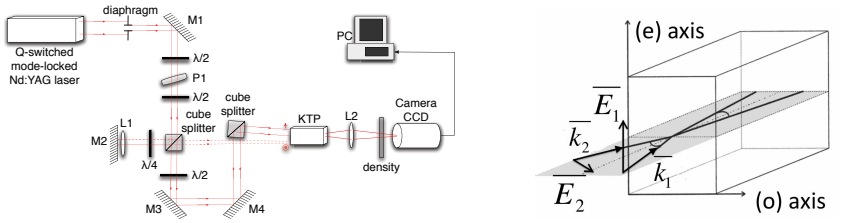

Fig. 5. Left, experimental set-up. M1, M2, M3, M4: mirrors. P1: polarizer. L1, L2: lenses. Right, schematic representation of the optical noncollinear configuration in the KTP crystal.

P_1, two independent beams with perpendicular linear polarization states. A half-wave plate placed before the prism serves to adjust the intensity of the two beams. By means of highly reflecting mirrors, beam splitters and lenses the beams are focused and spatially superimposed in the plane of their beam waist with a circular shape of $300\mu m$ and $6mm$, full width at half maximum in intensity, for the signal and pump waves respectively. A $L = 3cm$ long KTP crystal **(**$d = 3.29pm/V$**)** cut for type II second harmonic generation is positioned such that its input face corresponds to the plane of superposition of the two input beams.

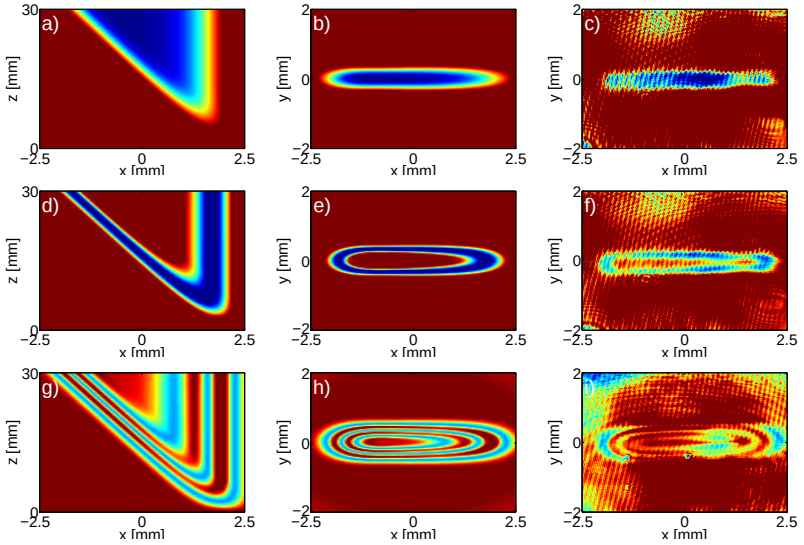

Fig. 6. Left column, numerical dynamics of the beam E_2 in the $x-z$ ($y=0$) plane. Central column, numerical, and right column, experimental results at the exit face of the KTP crystal presenting the spatial $x-y$ output profiles of E_2. Upper row, frequency conversion regime ($I_1 = 10MW/cm^2$, $I_2 = 0.03MW/cm^2$); central row, soliton triad generation ($I_1 = 50MW/cm^2$, $I_2 = 0.2MW/cm^2$); lower row, non-interacting soliton triad ensemble ($I_1 = 500MW/cm^2$, $I_2 = 5MW/cm^2$).

The crystal is oriented for perfect non-collinear phase matching between the signal and pump waves. The directions of the linear polarization state of the two beams are adjusted to coincide with the extraordinary and the ordinary axes, respectively, of the KTP crystal. The wave vectors of the input beams are tilted at angles of 3.6^o and 3.6^o (in the crystal) with respect to the di-

#144063 - $15.00 USD Received 11 Mar 2011; revised 9 May 2011; accepted 26 May 2011; published 23 Jun 2011

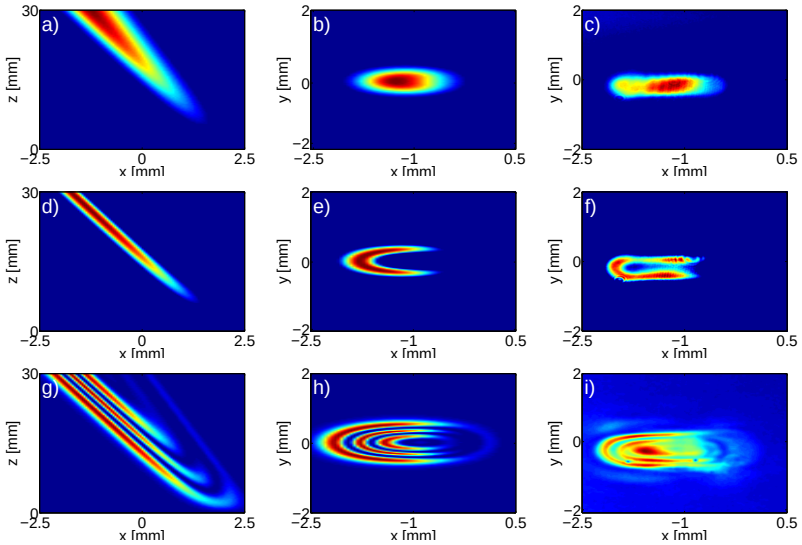

Fig. 7. Left column, numerical dynamics of the beam E_3 in the $x-z$ ($y=0$) plane. Central column, numerical, and right column, experimental results at the exit face of the KTP crystal presenting the spatial $x-y$ output profiles of E_3. Upper row, frequency conversion regime ($I_1 = 10MW/cm^2$, $I_2 = 0.03MW/cm^2$); central row, soliton triad generation ($I_1 = 50MW/cm^2$, $I_2 = 0.2MW/cm^2$); lower row, non-interacting soliton triad ensemble ($I_1 = 500MW/cm^2$, $I_2 = 5MW/cm^2$).

rection of perfect collinear phase matching for the extraordinary and the ordinary components, respectively (see Fig. 5). The idler second harmonic direction lies in between the input beams directions **(-1.16^o)**. With these values of parameters, spatial diffraction, group velocity mismatch and temporal dispersion were negligible. The spatial waves' patterns at the output of the crystal are imaged with magnification onto a CCD camera and analyzed. We use alternately different filters and polarizers to select either the IR or the green output.

Equations (1) describe the experimental spatial quadratic resonant interaction in the KTP. As spatial diffraction is negligible in the experiments, Eqs. (1) reduce to the integrable TWI Eqs. (2) in the ordinary $x-z$ plane ($y=0$ plane). In the $x-z$ plane (as well as in each plane parallel to $x-z$), the experimental set-up creates the two-dimensional environement to excite the predicted TWI soliton dynamics.

Indeed, we observed different regimes in the ordinary KTP $x-z$ $(y=0)$ plane as the intensities of the input signal and pump are varied in a suitable range (Figs. 6, 7). Left columns of Figs. 6, 7 show the numerical spatial evolution of the pump beam and the SF beam (which are the beams that best report the TWI soliton evidence) in the ordinary $x-z$ $(y=0)$ plane; central and right columns report, respectively, the numerical and experimental spatial output profiles of the beams in the $x-y$ $(z=L)$ plane. The numerical and experimental results are reported considering a spatial frame moving with the pump walk-off angle. At intensities $I_1 = 10MW/cm^2$, $I_2 = 0.03MW/cm^2$, the signal interacts with the pump and a SF beam at the second harmonic is generated. This regime corresponds to the well-known optical noncollinear second-harmonic frequency conversion (Fig. 6(a), 6(b), 6(c) and Fig. 7(a), 7(b), 7(c)). At intensities $I_1 = 50MW/cm^2$, $I_2 = 0.2MW/cm^2$, signal and pumb beams generate a stable bright-dark-bright solitary triplet (Fig. 6(d), 6(e), 6(f) and Fig. 7(d), 7(e), 7(f)). Increasing further input intensities we have observed the generation of two and three non-interacting bright-dark-bright

#144063 - $15.00 USD Received 11 Mar 2011; revised 9 May 2011; accepted 26 May 2011; published 23 Jun 2011

triads. Figures 6(g), 6(h), 6(i) and Fig. 7(g), 7(h), 7(i) show the generation of three non interacting bright-dark-bright triads ($I_1 = 500MW/cm^2$, $I_2 = 5MW/cm^2$). Figures 6(i), 7(i) report the first observation, to the best of our knowledge, of an ensemble of non-interacting TWI soliton triads.

5. Conclusions

We studied the dynamics of a spatial narrow beam at frequency ω_1 (the signal) and a quasi-plane wave at frequency ω_2 (the pump) which mix to generate a beam at the sum frequency (SF) ω_3 (the idler), when diffraction is negligible. Depending on the input intensities different nonlinear regimes exist. In this paper, the focus was on the generation and dynamics of an ensemble of TWI soliton triads. We predicted theoretically and demonstrated experimentally non–interacting triads ensemble in a KTP crystal.

Acknowledgments

The present research in Brescia is supported by Fondazione CARIPLO grant 2010-0595, in Limoges is supported by the VINCI program.

#144063 - $15.00 USD Received 11 Mar 2011; revised 9 May 2011; accepted 26 May 2011; published 23 Jun 2011